Probe Design and Construction

F. David Doty
Doty Scientific Inc., Columbia, SC, USA

1 INTRODUCTION

From the early days of NMR, the word probe (or probe-head) has been used to refer to the complete piece of equipment intimately associated with the sample (except the sample tube). For the simplest experiments, the probe consists of the mechanical structure required to hold the sample in the 'sweet spot' of the magnet, a coil surrounding the sample, a tuning capacitor, and an rf transmission line. However, most chemical problems of interest require control over the sample environment (temperature, electromagnetic irradiation, field gradients, pressure, orientation, and rotation), and apparatus associated directly therewith becomes a part of the NMR probe.

The modern NMR probe is a complex piece of apparatus designed to accommodate all of the environmental requirements of the NMR experiment. The radiofrequency (rf) portion often includes (a) an rf 'observe' channel optimized for highest signal-to-noise-ratio (SNR, or S/N, also called sensitivity) at the X-nucleus frequency, (b) a less efficient rf channel for heteronuclear decoupling (usually ^{1}H, except for indirect detection), and (c) another low-efficiency channel for magnetic field lock (usually ^{2}H). Variable temperature (VT) control is achieved with a resistive heater in a gas stream that flows over the sample. In high-resolution liquids probes, slow sample spinning (10-200 revolutions per second, Hz) about the B_0 axis to average out azimuthal inhomogeneity in B_0 is usually accomplished with a pneumatic system *external* to the probe, but high-speed sample spinning apparatus (200-50,000 Hz) for solids averaging techniques is an integral part of a solids probe.

One of the most demanding technical aspects of liquids probes is the requirement of extremely high B_0 field homogeneity (often better than one part per billion), but sometimes it is advantageous to be able to deliberately spoil the field homogeneity over precise time periods by applying field gradients. When very high gradients and fast switching are required, as in diffusion measurements or some microscopy magnetic resonance imaging (MRI), the gradient coils must be as small as possible and incorporated into the probe. However, for most MRI work, especially with samples larger than 40 mm, the gradient coils are external to the probe.

Another challenging technical requirement is often that of minimizing NMR background signals from construction materials that contain trace amounts of the nuclide of interest, particularly for highly sensitive proton (^{1}H) experiments. Other technical complications may stem from provisions for optical or microwave irradiation and operation at extreme temperatures. Automatic sample eject/load capability has been standard for more than three decades in liquids probes, and it is recently becoming available in solids probes. Addressing the often conflicting requirements of high sensitivity, high resolution, large spec-

tral bandwidth, low background signals, wide VT range, high-speed sample spinning, high-power decoupling, auto-sample exchange, and pulsed field gradients requires careful attention to a number of problems in materials science, physics, electrical engineering, and mechanical engineering.

The progress in increasing the performance of NMR probes over the past decade has exceeded the earlier expectations of many. The most significant, generally applicable contribution to increasing S/N in the past decade has been the introduction of cryoprobes (for liquid samples) in which the sample coil and capacitors are cooled to about 25 K while the sample may be near room temperature. Undoubtedly, significant advances in NMR probe technology will continue for quite some time.

2 GENERAL CLASSES OF NMR PROBES

2.1 Liquids Probes

Approximately 80% of NMR experiments are performed on high-resolution liquids probes designed for samples in axially aligned glass tubes in superconducting magnets using saddle-shaped rf coils or slotted resonators for signal reception.[1] They are often required to achieve spectral resolution of about one part per billion,[2, 3] perhaps on slowly spinning samples. A small fraction of their usage has been for *in vivo* experiments on small living animals or *ex vivo* or *in vitro* experiments on surgically removed tissues kept alive for short periods of time by perfusion with nutrients in saline solutions furnished by a flow system in the probe. Most multinuclear liquids probes prior to the early 1990s provided proton decoupling with multinuclear observe and deuterium lock, but since then the majority have been designed for inverse experiments (proton detection with X-nucleus decoupling). At present, high-resolution liquids probes are commercially available for experiments from -180^0C to $+500^0$C.

Most liquids probes today are supplied with a B_0 gradient coil, which is beneficial for measurement of diffusion coefficients, for solvent suppression, or for selection of specific coherences.[4] Their usage has grown rapidly in the past decade, especially because of the time savings they provide in two-dimensional NMR. Usually, this coil is capable of producing a gradient only along the z axis and of rather high magnitude. Such probes are often denoted Pulsed Field Gradient (PFG) probes.

Recently, cryogenic cooling of the sample coil and the critical capacitors in Cryoprobes have yielded S/N gains of up to a factor of four for low-loss samples near room temperature.[5] Most of these probes have utilized magnetically compensated aluminum-foil coils, cooled to about 25 K, as high-temperature superconductors (HTS) have presented numerous challenges, especially in resolution, that outweigh any advantage in conductivity compared to cold, high-purity aluminum. Cryoprobes, like their conventional predecessors, are available for triple resonance experiments with gradient coils at fields up to 21 T. (See also **Probes for High Resolution**.)

2.2 Solids Probes

The original (and simplest) probe for NMR of solid samples is the wideline probe, which is normally characterized as being able to generate 90^0 pulse lengths less than 3 μs (spectral excitation bandwidths greater than 80 kHz), sometimes by withstanding peak rf coil voltages in excess of 3 kV. Often they are double-tuned (DT) to permit cross polarization (CP) with high-power decoupling for increased sensitivity and resolution. Proton decoupling in solids often requires rf field strengths in the range of 50-150 kHz, an order of magnitude higher than normally possible in liquids probes, and this leads to severe rf heating of the sample in high-field magnets unless special ultra-low-E-field coils are used.[6]

Most solids probes today include high-speed Magic Angle Spinning (MAS) of the sample, primarily for line narrowing of spin-1/2 nuclei [7] and for removing broadening from bulk susceptibility variations in inhomogeneous semi-solid systems such as tissues. Rotational rates in the range of 2000 to 7000 "Hz" (revolutions per second) are generally sufficient for the mobile components in semi-solids, but spinning rates up to 70 kHz are needed for improved narrowing of ^{1}H lines in some solids. High-speed sam-

ple spinning technology has advanced steadily over the past two decades, and 4 mm silicon-nitride rotors are now routinely and safely spinning over 26 kHz with samples of moderate density.

Dynamic Angle Spinning (DAS) and Double Rotation (DOR) have been provided for quadrupolar nuclei, though these techniques have largely been supplanted with high-power multi-pulse techniques. When sufficiently large single crystals of the sample can be grown, high-resolution spectra and the chemical shift tensor can be obtained using a single-crystal probe that includes a suitable goniometer and crystal orientation mechanism. (See also *Solid State NMR Probe Design*.)

2.3 Microimaging Probes, Coils, Resonators, Platforms, and Modules

Microimaging (μMRI) probes began very much like conventional liquids probes with the addition of a 3-axis gradient coil. Nowadays, most microimaging is done in horizontal-bore magnets, as the vast majority of the applications involve small animals, and their handling is much easier in the horizontal bore. The 3-axis gradient coil is considerably more complex and expensive that the rf "coil", so there is strong motivation to use a single-size gradient coil with a variety of interchangeable, specialized rf coils, especially in horizontal-bore magnets.

The MRI rf "coil" seldom bears any resemblance to a coil in the original sense of this word, but the name survives from historic origins, as the first rf detectors were solenoidal coils. Today, most MRI rf resonators are birdcages [8] or modified, segmented saddle coils,[9] often with paralleled conductor foil paths with insulated cross-overs, known as "litz coils", from analogy to litz wire.[10] The combination of the rf resonator and animal handling apparatus is often called a "platform" if it is a rather open structure, or a "module" if mostly enclosed, but both are also known simply as "coils" to many users and "probes" to others. Microscopy *in vivo* probes often include surface coils for improved localized signal reception. Phased Arrays, which have been widely used for more than a decade in whole-body MR, are also beginning to find applications in μMRI,[11] and cryogenically cooled MRI surface coils are beginning to be evaluated for mouse brain.[12] (See also *Radiofrequency Systems and Coils for MRI & MRS*, and *Surface and Other Local Coils for In Vivo Studies*.)

3   HISTORICAL PERSPECTIVE ON NMR PROBES

Through the late 1960's 'NMR' implied 'proton NMR of liquids' unless specifically stated otherwise, and multinuclear probes were unheard of. There was a rather widespread misconception that sensitivity increased linearly with coil inductance, even though the early classic treatments.[13, 14] were sound. High-inductance solenoids (1-50 μH, compared to 30-200 nH for modern probes) wound around the sample tube could be used for efficient reception in the transverse field of the electromagnet, and audio field-modulation coils were needed to shift the detection frequency above the $1/\nu$ noise region of the phase-sensitive video detector. The orthogonal Helmholtz transmit coils could be driven with low-power (milliwatt) oscillators for most continuous wave (CW) techniques, and the transmit/receive coils were carefully isolated using Faraday shields and tuning paddles. Since low-impedance preamplifiers with low noise figures were not available, it was best to include the first stage of the preamplifier in the probe and match it (usually 300-2000 Ω) directly to the receive coil.

Although many time domain pulsed NMR experiments were performed in the first two decades of NMR for relaxation studies, the explosion of NMR techniques awaited the application of Fourier Transform (FT) by Richard Ernst in 1966 to the time domain data to obtain the complete frequency domain spectra in a single free induction decay (FID). The increase in sensitivity was comparable to the ratio of the total spectral width to the narrowest line in the spectrum - often two or three orders of magnitude.[15, 16] (See also *Fourier Transform Spectroscopy*.)

Field shimming (homogenizing) was extremely crude and tedious prior to Golay's development of the theory and practice of orthogonal shim coils.[17] (The name comes from the original homogenization technique of placing small pieces of metal foil, shims, under the edges of the magnet pole caps.) With the

advent of FT NMR came more incentive to obtain higher resolution because of its dramatic impact on sensitivity. Ultra-high purity (99.999%) copper receive coils with precision magnetic compensation [2,3] and Varian's sample spinner mounted on top of the probe quickly became standard. An external lock employing a sealed sample and separate coil (usually tuned to ^{19}F or ^{2}H) beside the sample coil was used to stabilize the field.[18] (See also ***Shimming of Superconducting Magnets***.)

The probe rf circuitry was also quickly impacted by FT NMR. To excite the entire spectral width with large Helmholtz coils at 60 MHz required 10-100 watts and generated several kilovolts across the coil, so impedance matching to the transmit circuit became important. The increase in sensitivity from FT NMR opened up the field of multinuclear NMR, especially ^{13}C and ^{31}P.[19] The advantages in resolution and sensitivity provided by proton decoupling required double resonance circuits, which made it more difficult to use separate transmit/receive coils, and double-tuned single-coil circuits with transmit/receive duplexers began to appear.[20] It is fair to say that modern NMR probe technology was ushered in by David Hoult in 1976 with his transparent analysis of SNR based on the obscure concept of reciprocity.[21] Today, separate transmit/receive coils survive only in single-resonance MRI where the high rf homogeneity afforded by a large transmit coil is beneficial and small surface coils are optimum for reception.

4 RF ENGINEERING – BASICS

Basic rf engineering has been treated in a number of excellent texts,[22, 23] but the probe engineer also needs a working understanding of some of the more advanced concepts in electromagnetic field theory.[24, 25] NMR signal reception is different from (and simpler than) antenna theory in that antennas are designed to receive electromagnetic waves in the far-field limit whereas NMR probes are designed to sense magnetic fields in the near-field limit. While the rf circuits in NMR probes can usually be approximated with simple circuits and analyses, the critical importance of the probe to the total spectrometer performance justifies a level of detailed field and efficiency analysis seldom encountered outside of NMR probes. At least one text book [26] and a number of articles [6, 21, 27-40] have presented excellent treatments of general NMR probe design issues over the past three decades. A summary of basic NMR probe electronics follows.

4.1 Capacitance

Capacitance (farads) is defined as electric charge per volt (Q/V), and capacitive energy storage is equal to $CV^2/2$. Stray capacitance can often be estimated to sufficient accuracy from the expression for the parallel-plate capacitor C_p of area A (m^2), separation distance d (m), and dielectric constant k_d,

$$C_p = \frac{k_d \varepsilon_0 A}{d} \tag{1}$$

or from the expression for the low-frequency capacitance of a coaxial capacitor [28] of length h, dielectric outside diameter d_o, and dielectric inside diameter d_i,

$$C_c = \frac{2\pi k_d \varepsilon_0 (h + d_o)}{\ln(d_o / d_i)} \tag{2}$$

where ε_0 is the permittivity of free space, 8.84 pF/m. Parallel capacitors add linearly ($C_T = C_1 + C_2 + ...$), while series capacitors add reciprocally ($C_T^{-1} = C_1^{-1} + C_2^{-1} + ...$).

.

4.2 Inductance

The simplest definition of inductance L (henrys) comes from Faraday's law of induction − the induced voltage divided by the rate of change in current, *di/dt*. For inductance calculations, the most practical 'definition' follows from the energy equation

$$U = i_T^2 L / 2 \qquad (3)$$

where U is the total energy in the magnetic field (the integral of $B^2/2\mu\mu_0$ over all space) and i_T is the current at the pair of terminals generating the magnetic field B. (We follow popular usage of denoting the magnetic flux density or induction field B (T) as the 'magnetic field' and $H = B/\mu\mu_0$ as the field intensity (A/m), where μ is the relative permeability of the material.) For all NMR probes, μ is always unity. The permeability of free space μ_0 equals 4π x 10^{-7} H/m.

The inductance of the finite, multiturn, single layer rf solenoid of Figure 1 with constant pitch, integral number of turns, and high surface coverage is given in nH, for dimensions in mm, by the following expression:

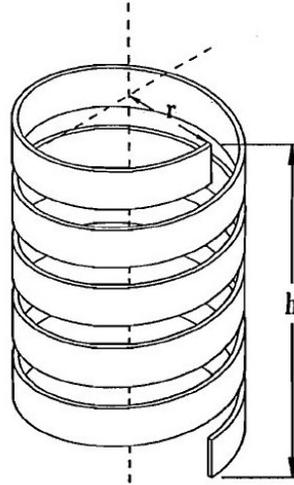$$L_S = \frac{4n^2 r^2 (1 - 0.2 / n)}{h + 1.2 r^{0.9}} \qquad \text{[mixed]} \qquad (4)$$

Figure 1　A five-turn solenoid

where n is the number of turns (Figure 1 has five turns), h is the overall axial length, and r is the effective inside radius, which for round wire is approximately equal to the inside coil radius plus 10% of the wire diameter. The last term in the numerator corrects for the fact that the helix makes the effective coil length a little less than the overall length. The above expression is usually correct to within several percent for h/r >0.2. For the loop-gap resonator [6, 41] (a single-turn solenoid, also called a split ring), the helix correction term is dropped, and the coefficient changes to 3.9 to correct for current concentrating at the ends of the ring. Higher order corrections for multi-turn coils with low surface coverage can be added.

Lead (parasitic) inductance may be estimated by calculating the inductance of a loop-gap resonator having length equal to the diameter of the lead wire and $r^2 = A_C/\pi$, where A_C is the area enclosed by the loop formed by the leads. Sometimes lead inductance is better estimated from the expression for the inductance L_C of a coaxial transmission line:

$$L_C = \frac{\mu_0 h}{2\pi} \ln \frac{d_o}{d_i} \qquad (5)$$

Clearly from equation (5), series inductors add like resistors ($L_T = L_1 + L_2 + ...$); likewise, parallel inductors add reciprocally ($L_T^{-1} = L_1^{-1} + L_2^{-1} + ...$)

.

4.3 Single Resonance Circuits

4.3.1   Power

Figures 2 and 3 illustrate the basic RLC series and parallel circuits respectively. The losses in the series RLC circuit of Figure 2 are best represented by the total effective series resistance R_s (from the coil, capacitor, leads, etc.). For the parallel circuit of Figure 3, the losses may be represented more conveniently by a total effective parallel resistor R_p. In both cases, the basic equations from AC circuits apply for rms power P and peak power P_P. (Power is assumed to be rms unless denoted otherwise.)

$$P = \frac{P_P}{2} = \frac{i_P^2 R_s}{2} = \frac{V_P^2}{2R_p} \tag{6}$$

Power ratios are often expressed in dB, 10 log(P_2/P_1), and power is often expressed in dBm, defined as dB relative to a milliwatt:
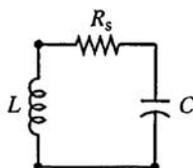
$$\text{dBm} \equiv 10 \log(1000P) \tag{7}$$
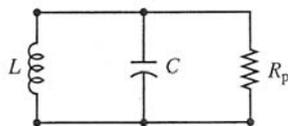

Figure 2   Series RLC circuit

Figure 3   Parallel RLC circuit

In practice, peak-to-peak voltages ($2V_P$) are usually measured on an oscilloscope, and the measurements are significantly influenced by harmonic distortion, VSWR (Voltage Standing Wave Ratio), loading, and oscilloscope bandwidth. Most conventional liquids probes are excited with ~100 W pulses of 10-80 μs at the observe frequency at duty cycles below 0.1% while they are driven with ~10 W at the decouple frequency at duty cycles below 50%. Solids probes typically see LF pulses of 200-400 W with duty cycles up to 1% while irradiating with HF power of 50-300 W at duty cycles below 30%. Whole-body MRI probes are usually driven with 1-5 kW at duty cycles below 0.5%.

4.3.2   Resonance

Since charge (q) equals CV and $i=dq/dt$, a capacitor reaches a steady-state (monochromatic) reactance X_C (analogous to resistance, V/i) of $1/j\omega C$ after several RC time-constants, where j is the imaginary unit, $\sqrt{-1}$. Likewise, since $V=-Ldi/dt$, an inductor has time constant L/R and reactance $X_L=j\omega L$. For the normal high-Q condition, resonance occurs when the inductive reactance X_L plus the capacitive reactance X_C equals zero. (Often the phase is omitted for convenience, but it must be remembered that the voltage phase in the inductor leads by 90^0 while in the capacitor it lags by 90^0 relative to that in the resistor.) Hence,

.

$$\omega_0 = \frac{1}{\sqrt{LC}} \tag{8}$$

At resonance, the series impedance of the series RLC circuit is R_s (since $X_L + X_C = 0$) and the parallel impedance of the parallel RLC circuit is R_p [since $(X_L X_C)/(X_L + X_C) = \infty$]. For the isolated (unmatched) LC circuit with lossless capacitors and a coil of quality factor Q_{0L}, the following relationships are readily derived:

$$R_p = Q_{0L} X_L \tag{9}$$

$$R_s = X_L/Q_{0L} = R_p/Q_{0L}{}^2 \tag{10}$$

4.3.3 Matching, Q_T, Q_L, and Q_U

Since X_L is typically 20-200 Ω, R_S is usually less than 1 Ω and R_P is generally greater than 2000 Ω. For efficient coupling to the transmitter (and preamplifier), the resonant circuit, transmission lines, preamplifier, and transmitter must all be matched to approximately the same impedance, although mismatches of up to a factor of two are often unimportant and deliberate mismatching is sometimes extremely beneficial.[34] The most common impedance is 50 Ω (except in the television industry, where it is 75 Ω). Figures 4 and 5 illustrate two basic methods of impedance matching: shunt inductor and series capacitor.
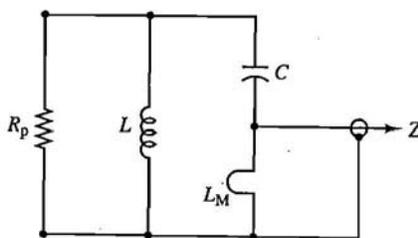

Figure 4   Shunt inductive matching circuit

The inductive matching technique has the advantage of not requiring a second high-voltage capacitor, but the matching range is limited by the difficulty of adjusting very small inductors. The required shunt inductor (for $R_p \gg Z_0$) is

$$L_M = L_T \sqrt{\frac{Z_0}{R_p}} \tag{11}$$

where L_T is the total series inductance ($L_S + L_M + $ leads) and Z_0 is the transmission line characteristic impedance – normally 50 Ω. The resonant frequency is calculated from L_T and C. A similar expression may be derived for shunt capacitive matching.[34]

The series capacitive matching circuit simplifies multinuclear (broadband) tuning requirements, as high voltage (HV) variable capacitors are readily available. The required match capacitance (again, for $R_P \gg Z_0$) has reactance X_{CM} given by

$$X_{CM} = \sqrt{R_p Z_0} \tag{12}$$

and rms current equal to that in the transmission line, $\sqrt{P/Z_0}$. In practice, some combination of capacitive and inductive matching is often used, and capacitive voltage division is often employed to reduce the demands on the matching variable capacitor.[42] Properly 'pruned' transmission lines can also be used to transform impedance [31] (see also, *Probes for Special Purposes*).

It is important to be more careful about the definition of Q than has often been the case in the NMR, MRI, and EPR literature – a factor-of-two matters! The early tradition in these fields was to report

.
the isolated Q_0 for a resonator − i.e., the value obtained with extreme under-coupling, as obtained in the limit of a very small series match capacitor or a very small shunt match inductor. One can define a Q_T for the isolated tank circuit consisting of a coil with losses according to eq. (10), a capacitor with losses similarly described by Q_C, and a sample with losses defined by Q_S:[6, 33]

$$\frac{1}{Q_T} = \frac{1}{Q_C} + \frac{1}{Q_{0L}} + \frac{1}{Q_S} \, . \tag{13}$$

When the tank circuit is impedance matched to a transmitter or preamp, the circuit Q is halved, as the preamp or transmitter impedance, for the parallel tank case, is transformed to an impedance equal to R_P and in parallel with it, and similar reasoning applies to the series tank. This matched tank Q is now customarily denoted Q_L, and it is equal to $Q_T/2$. Outside the NMR, MRI, and EPR literature, it has been customary for quite some time to equate "Q" with Q_L:

$$Q_L = \omega/\Delta\omega_3 = Q_T/2 \, , \tag{14}$$

where $\Delta\omega_3$ is the -3dB width of the S11 response for the matched circuit. Q_T is also given by $\omega/\Delta\omega_7$, where $\Delta\omega_7$ is the -7dB width of the S11 curve for the matched circuit.[29] A reflectance bridge may be calibrated experimentally for Q_T measurement with a 21 Ω or a 119 Ω load, as these have an S11 of -7dB for a 50 Ω line.[29] There is an increasing tendency to report Q_L in the NMR and MRI coil literature, and Q_U is sometimes used to refer to Q_L for the matched tank without a sample. (Note that Q_L no longer means "sample-loaded Q_T", as it did in the early days.)

For the hi-Q solenoid (heavy wire, high surface-coverage, $h \approx 4r$), Q_{0L} is found to be given approximately (in mixed units) by

$$Q_{0L} \approx 12 \, r \sqrt{f} \quad [\text{MHz}^{1/2}\,\text{mm}^{-1}] \tag{15}$$

for frequencies far below self resonance. (The dependence on h/r is rather small.) In practice, Q_T is likely to be about half of the above limit, and the difference between heavy round wire and closely spaced flat wire is small.[43]

5 SIGNAL-TO-NOISE RATIO AND B₁

5.1 Magnetization and the NMR Signal

The NMR voltage signal S from a sample with susceptibility χ, with nuclear spins precessing at angle ϕ in magnetic field $\boldsymbol{B}_0$ at angular frequency ω, detected by a coil that generates a circularly polarized (rotating) transverse field $\boldsymbol{B}_1(\mathbf{r})$, over the sample volume V_S for current i, may be shown from the principle of reciprocity[21] to be

$$S = \frac{\chi B_0 \omega}{\mu_0 i} \int_S \sin\phi \, B_1(\mathbf{r}) \, dV \tag{16}$$
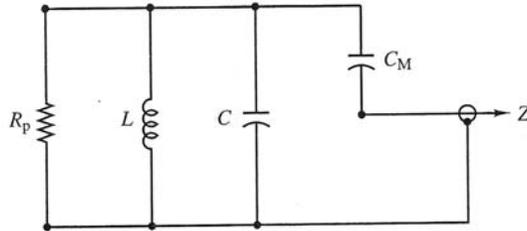

Figure 5   Series capacitive matching circuit

Simply put, the receiver coil need only be analyzed as a B_1 transmitter. For a uniform B_1 generated by current i, immediately following a 90^0 pulse,

$$S = \frac{\chi B_0 \omega B_1 V_S}{\mu_0 i} \tag{17}$$

The equilibrium magnetization M_0 is given by [13, 18]

$$\mathbf{M}_0 = \frac{\chi \mathbf{B}_0}{\mu_0} = \frac{n_s \gamma^2 \hbar^2 I_x (I_x + 1) \mathbf{B}_0}{3 k_B T_S} \tag{18}$$

where n_s is the number of spins at resonance per unit volume, γ is the magnetogyric ratio, I_x is the spin quantum number, k_B is Boltzmann's constant, T_S is the sample temperature, and $\hbar = h/2\pi$ where h here is Planck's constant.

5.2 Thermal Noise

The Johnson (thermal) rms noise voltage N from a resistor R_E for filter bandwidth Δv (not v/Q) is [13, 14]

$$N = (4 R_E k_B T_n \Delta v)^{1/2} \tag{19}$$

where T_n is the temperature of the resistor. (For $R_E = 50\ \Omega$, $N = -168$ dBm Hz$^{-1/2}$.) The effective series resistance of the loaded circuit is often best determined from X_C/Q_T. Other noise sources (interference, triboelectric, spurious, shot, microphonic, radiation, preamplifier) can usually be made negligibly small with careful engineering.[29] We return to the subject of noise in a little more detail after calculating S/N.

The preamp also often adds significant noise, as its noise figure (NF) is often about 1 dB, corresponding to a noise temperature T_P of 75 K.[29] This is most easily handled by adding its noise temperature to the resistor noise temperature in eq. (19).[44] When the total noise comes from multiple losses at different temperatures, the various noise powers add.

5.3 The Rotating B_1

A linearly polarized oscillating magnetic field $2B_1$ (as in a solenoid) may be decomposed into the sum of two oppositely rotating circularly polarized fields, each of magnitude B_1. One of these components can be used to drive NMR precession within a bandwidth approximately equal to its magnitude (in Hz) if it is transverse to B_0; the other has no effect on NMR precession, as its frequency in the rotating frame is -2ω. From the Biot-Savart law,[24] B_1 at the center of a solenoid is given by

$$B_1 = \frac{\mu_0 n i}{2h\sqrt{1 + 4(r/h)^2}} \tag{20}$$

Using equations (3), (6), and (10), it may be shown that $U = P Q_T/\omega$; and B_1 may be expressed as follows for the infinite solenoid:

$$B_1 = \left[\frac{\mu_0 P Q_L}{\omega V_C} \right]^{1/2} \tag{21}$$

where V_C is the coil volume. [Adding the term $1 + 4(r/h)^2$ in the denominator inside the brackets of equation (20) improves accuracy for short solenoids.]

Saddle coils (commonly, but incorrectly, called Helmholtz coils;[24] more properly they could be called Ginsberg[45] or Golay[17] coils) and slotted resonators[1, 9] are better suited for liquids NMR in superconducting magnets, as they generate a transverse B_1 while allowing axial access. Moreover, their axial

.

symmetry makes it easier to obtain high B_0 homogeneity. Their Q is usually about half that of a solenoid of similar volume, and possibly even lower for orthogonal double resonance operation.

For *any* coil in which sample dielectric resonances are not significant, *average* B_1 in Gauss over the usable volume may be expressed in mixed units by the following:

$$\langle B_1 \rangle \cong \beta \sqrt{\frac{\eta_E P Q_T}{f V_C}} \qquad \text{[mixed]} \qquad (22)$$

where β is a dimensionless function of coil geometry, f is in MHz, V_C is in ml, and η_E is the rf efficiency − the fraction of power delivered to the rf sample coil and sample.[28] The rf efficiency η_E is usually greater than 0.9 for single-resonance circuits at low fields, but it may be less than 0.2 for triple resonance at high fields.[6] The above equation may become slightly more accurate if η_E is defined as the fraction of power dissipated just in the sample coil and Q_{OL} is used in place of Q_T, but these parameters are more difficult to determine accurately, except possibly with well validated full-wave numerical methods. [6]

For very lossy samples, optimum h/r is the largest permitted by space constraints, and $\beta = \sqrt{10}$ for the infinite solenoid. For MAS, the optimum h/r is often ~4, and β then is ~2.2 when the coil is at the magic angle. For saddle coils and slotted resonators, β ranges from 0.8 to 1.5, depending on surface coverage, subtended angle, and the ratio of height to diameter; and it is typically between 1 and 2 for the birdcage.[33]

A magnetic filling factor η_f may be defined by:

$$\eta_f = \frac{\int B_1^2 dV}{\mu_0 U} \qquad (23)$$

where the integration is over the sample volume V_S. Note that this is the ratio of the energy in the positive rotating circularly polarized field to the total magnetic energy, and B_1 is a constant field, not an oscillating field, a point that has previously caused some confusion.[33] From equations (3), (10), (22), and (23) comes a useful relationship:

$$\eta_f = \frac{\beta^2}{20} \frac{V_S}{V_C} \qquad (24)$$

There is a simple method for experimentally measuring magnetic filling factor.[46, 47] If a small metal sphere of volume V_M is introduced into a homogeneous circular polarization sample region of volume V_S, the magnetic filling factor is given simply by:

$$n_f \cong \frac{4 f_\delta V_S}{3 f_0 V_M}, \qquad (25)$$

where f_δ is the shift in resonant frequency f_0.[33] The expression is accurate only when the test ball is in a uniform transverse magnetic field with low electric fields and negligible axial magnetic field. Even with these caveats, our experience is that the above expression tends to overestimate mean η_f by ~20%.

5.4 SNR

From the above, the SNR from a single 90^0 pulse with an optimum filter $[1/(\pi \Delta v) = T_2^*$, the effective transverse relaxation time, and $\Delta v < \omega/2\pi Q_L]$ can be shown to be:

$$S/N = \left[\frac{\hbar^2 \sqrt{2\pi\mu_0}}{12 k_B^{3/2}} \right] \left[\frac{n_s \gamma I_x (I_x + 1) \sqrt{T_2^*}}{T_S \sqrt{T_n + T_P}} \right] \left[\sqrt{\eta_E \eta_f Q_L V_S} \right] \omega^{3/2} \qquad (26)$$

A factor of 2 in the denominator arises because S is the initial peak signal voltage that decays with time-constant T_2 and N is the rms noise voltage. The numerical coefficient in eq. (26) differs from a previously published expression by $\sqrt{2}$ because of the changed definition of Q_L. The product of the two bracketed terms is 6.6E-5 $(s/m)^{3/2}$ for protons in water with $T_2^* = 1$ s, $T_S = 300$ K, and $(T_n + T_P) = 370$ K.

A very useful simplification of equation (26) is the following for given NMR conditions (sample, γ, $\boldsymbol{B}_0$, T_S, T_2^*, method) in probes with sample coils at room temperature and negligible preamp noise:

$$S / N \propto \frac{V_S}{\tau_{90} \sqrt{P}} \tag{27}$$

where τ_{90} is the mean 90^0 pulse width obtained over sample volume V_S with power P applied to the probe from the same point where the preamp is connected. However, it is important to note that the above, which has been called a practical definition of the principle of reciprocity,[48] is not sufficient in evaluating either cryoprobes or preamp-decoupled phased-array coils, and it is seldom as simple as inserting $\sqrt{T_n + T_P}$ into the denominator of eq (27).[49] (See also, *Sensitivity of the NMR Experiment*.)

5.5 Minimizing Losses

For small samples, the Q_T is usually dominated by coil resistance. However, above 400 MHz it may be dominated by capacitor losses in many solids and liquids NMR cases unless care is taken in their selection, and it may be necessary to parallel several low-value capacitors for sufficiently low capacitor losses. (Q_C is usually approximately proportional to $C^{-0.8} f^{-1.5}$.) Very recently, finite element software has developed to the point that it can accurately calculate surface current distributions and all losses (conductor surface, sample, radiation, shields, capacitors, etc.) in the most complex coil and sample arrangements in a reasonable period of time – perhaps several hours.[6, 51] This has rendered obsolete much of the earlier analytical and approximate methods, though many contain valuable insights and data.[43]

For large, lossy samples, Q_T and T_n are dominated by sample losses. Dielectric losses from $\boldsymbol{E}$ fields in the sample can often be reduced by decreasing the coil inductance and increasing the capacitance,[50] as this reduces the so-called conservative electric field, the part that does not come from $d\boldsymbol{B_1}/dt$.

When conservative electric fields are fully minimized, a useful estimate of Q_S for cases well below dielectric resonances (i.e., when the product of frequency and sample diameter is below 10 MHz-m) is given by

$$Q_S \approx \frac{32\pi \, \xi \, V_C}{\mu_0 \eta_E \sigma \beta^2 \omega V_S^2} \tag{28}$$

where σ is the sample conductivity and ξ is the mean flux path length in the sample.[33] (A typical mean tissue resistivity is ~2 Ωm, which is similar to 50 mM saline at high fields.) The above equation is approximately equivalent to more specific expressions given by Carlson and Macovski.[52, 53] A precise calculation of the power P_S dissipated in the sample is possible using advanced, full-wave software:

$$P_S = \tfrac{1}{2} \int \sigma E^2 dV \tag{29}$$

The ratio Q_U/Q_L has frequently been used as a figure-of-merit for coils in MRI, but this has limited utility when the conservative E field is not fully minimized or when rf fields have substantial magnitude in lossy sample material beyond the homogeneous region of interest. Equation (27) provides a much better figure-of-merit.

The 'birdcage' resonator of Edelstein et al. made quadrature coils practical for generating a single rotating $\boldsymbol{B}_1$.[8, 54] Liquids and solids NMR find few applications for quadrature rf coils, often because coil losses dominate or because of the susceptibility matching challenges in liquids NMR probes. However, in MRI, when inductive sample losses dominate, quadrature coils offer up to a 40% improvement in SNR. For an advanced treatment of the birdcage resonator, the reader is referred to the article by Tropp.[30] (See

also ***Birdcage and Other High Homogeneity RF Coils for Whole Body Magnetic Resonance,*** and ***Radiofrequency Systems & Coils for MRI & MRS****.)*

6 DOUBLE RESONANCE

Two saddle coils, rotated 90^0 about the $\boldsymbol{B}_0$ axis provide a convenient method of doing double resonance NMR with good isolation. However, only the innermost coil can have optimum filling factor, and sometimes it is beneficial to have the same spatial distribution of the two rf fields, $\boldsymbol{B}_1$ and $\boldsymbol{B}_2$. Also, triple- or quadruple-resonance NMR experiments are often useful. Thus, it is often desirable to double-tune or triple-tune a single sample coil.

The number of modes in a resonant circuit will generally be equal to the number of unique inductors or capacitors, whichever is fewer. (Transmission lines may count as either.) It is sometimes necessary to add additional inductors or capacitors to improve isolation or to achieve balance at the frequencies of interest, although this can complicate tuning and produce extraneous modes.[55, 56]

A common double-tuned circuit, shown in Figure 6, has been analyzed by several authors.[28, 29, 57] It has an HF parallel mode and an LF series mode. The efficiency at the HF is increased by *decreasing* L_S/L_H, where L_S is the sample coil inductance and L_H is the HF tuning coil inductance. On the other hand, efficiency at the LF is increased by *increasing* L_S/L_H. In principle, if the losses in L_H and the tuning capacitors can be made vanishingly small compared to sample losses, efficiency can approach 100% at both frequencies.[58] Rise time, however, will be degraded (because Q_T must increase), but this is seldom significant for *in vivo*. Efficiencies at HF and LF are typically 30-40% and 60-80% respectively.
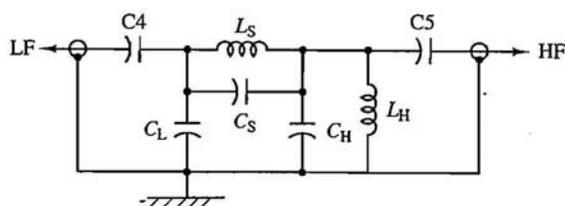

Figure 6   Double resonance circuit

From equations (22) and (26), B_1 and S/N are degraded only as the square root of the efficiency, but this is still quite significant. It becomes even more significant in high-field triple resonance, where efficiencies on two of the three channels may be below 25% [6]. It has recently been shown that in such cases cryogenic cooling of the critical tuning elements (coils and capacitors) external to the sample coil can increase effective "efficiencies" (from a S/N perspective) by more than a factor of two, as both the resistances and the noise temperatures of these losses are reduced.[49]

While the insights provided by simplified circuit analyses are valuable, the task of analyzing and optimizing efficiency in complex circuits at high frequencies is best addressed using linear circuit simulators, such as ARRL Radio Designer, SPICE, GENESYS, or Ansoft Designer.[59] All component leads more than a few millimeters in length are usually modeled individually as short transmission lines of appropriate propagation factor, attenuation constant, impedance, and length. The coils are modeled with appropriate, frequency-dependent Q_{OL}, and the capacitors may be modeled with appropriate self inductance and frequency-dependent series resistance without too much difficulty. (For example, a 1 kV 10 pF TEMEX CHB chip capacitor would be modeled as an ideal 10 pF capacitor in series with a 1 nH inductor having $Q_{0L}=30$ at 400 MHz and this Q_{0L} proportional to $f^{1/2}$.) It can be shown that, for a given sample coil, the S/N at each frequency is optimized by maximizing the voltage across the sample coil for a given excitation voltage (or power) at the matched port at the respective frequency, irrespective of the complexity of the circuit, when all the losses are at the same temperature.[60] When some losses are at significantly different temperatures, the various resistors (losses in the coils, capacitors, sample) must be scaled in proportion to their absolute temperatures.[49, 60]

7   DECOUPLER HEATING

RF heating of the sample during ^{1}H decoupling has long been recognized as a challenge to be dealt with in saline liquids NMR, especially with larger samples at higher fields; and the Alderman/Grant coil has been the gold-standard for liquids NMR at high fields for nearly three decades.[50] More recently, several approaches have been pursued for double and triple-resonance solids MAS applications, where sample volumes are usually much smaller but decoupling field strengths are much higher.

The "scroll coil"[61] appears to have about one-fifth the dielectric heating of a typical, small MAS solenoid, but its extra low inductance (as needed to limit the self resonance) leads to lower S/N in multi-tuned coils, though it is ideally suited for single resonance. The "cross coil"[62, 63] (XC) appears to offer approximately another factor of two drop in dielectric heating for the 4 mm case.[6] In this approach, the XC is used for ^{1}H only, and an outer solenoid is double tuned for the mid-frequency and low-frequency channels. This approach has also been shown to have additional useful attributes for triple-resonance high-field MAS, especially if axis re-orientation is desired for auto sample eject.

8   CONSTRUCTION MATERIALS AND TECHNIQUES

Although B_0 homogeneity specifications sound frighteningly stringent, the capability of orthogonal shim systems is such that only in the immediate vicinity of the sample is magnetic susceptibility critical. Austenetic stainless steels (with SI volumetric susceptibility $\chi_V = \mu - 1 \approx 0.003$) can often be used for thin-walled dewars surrounding the sample region and for dewared transfer lines, although glass is preferred if space permits. It is, of course, desirable to minimize the amount of shimming effort required when the probe is changed, so low-susceptibility construction materials and thin sections are preferred. The magnetic susceptibilities of the components immediately above and below the sample region (in the B_Z direction) are more significant, and axial and azimuthal symmetry are both helpful.[3, 64, 65]

The specified iron limit in the common high-purity copper grade C10100 (also commonly called OFHC) is 10 ppm, and it seems to typically be ~4 ppm. The solubility of iron in copper at 200^0C is 13 ppm,[66] so precipitation into ferromagnetic inclusions at grain boundaries is improbable. However, cutting copper with steel tools often leaves enough iron contamination worked into the surfaces to cause serious ferromagnetism. Hence, it is important to use ceramic cutting tools when working on sample coils.

The common aluminum alloys[67] 6063-T6 (0.7% Mg, 0.4% Si, up to 0.3% Fe) and 6061-T6 (1% Mg, 0.6% Si, 0.3% Cu, 0.3% Cr, up to 0.7% Fe) are usually acceptable for thin shield cylinders and support structure since the iron is usually in a non-magnetic phase ($FeAl_3$ or Fe_2Al_7),[66] but they often present acoustic ringing problems below 15 MHz.[68] The iron content in the readily available tin bronzes (more often called phosphor bronzes, as they may contain a trace of phosphorus), such as C51000 [94.8% Cu, 5% Sn, 0.2% P, 0.1% Fe (max.)] does not usually present a problem, as the iron is bound up in a tin-rich phase which is not ferromagnetic.[3] However, zinc brasses must be checked carefully if they are to be used within $r_b/3$ of the sample, where r_b is the bore radius, as they are likely to have ferromagnetic inclusions; and aluminum bronzes are usually best avoided.

The critical importance of high-integrity ground connections throughout multiple-resonance probes cannot be overemphasized. Welding, press-fits, and solder joints are preferred over silver-filled epoxy and silver paint.[29] The external shield cylinders are often tin or chromium plated or anodized for an aesthetically pleasing finish that also helps eliminate variability in grounds. Figure 7 illustrates three NMR solids probes: a narrow-bore MAS probe compatible with limited cryogenic cooling, a wide-bore SAS probe and a wide-bore high-temperature MAS probe (from left to right respectively).
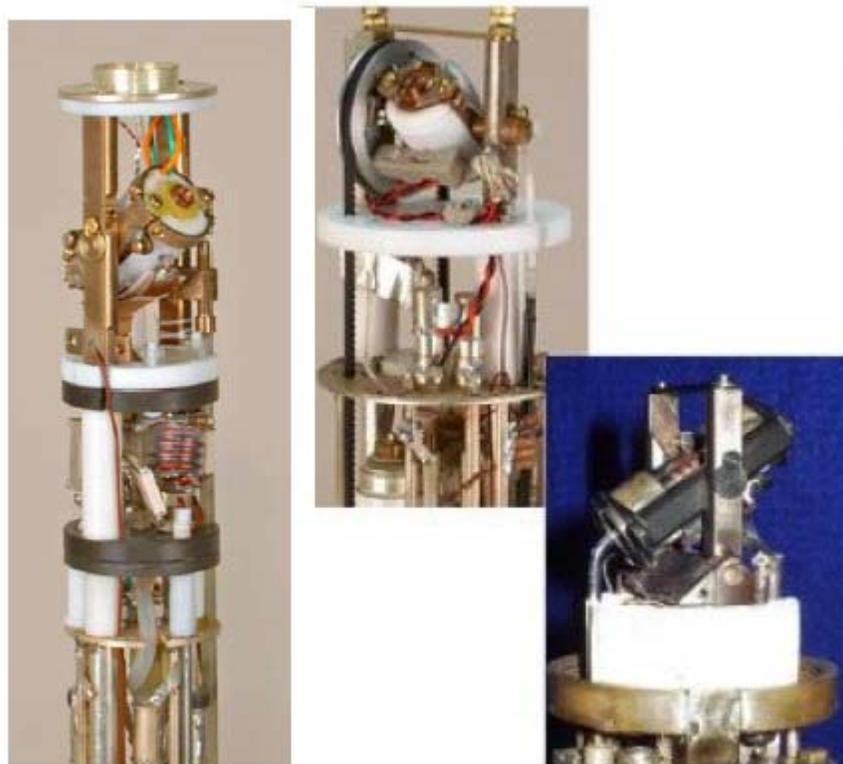
Figure 7   Three NMR Solids probes

Quartz is usually selected for coil forms in high-field magnets because of its lower dielectric loss, even though its magnetic, mechanical, and acoustic properties are inferior to those of pyrex. Acoustic ringing in quartz, macor, and ceramic capacitors may cause problems at frequencies up to 50 MHz. Zirconia has often been used in MAS probes for rotors and stators because of its superior mechanical and magnetic properties. Silicon nitride, Si_3N_4, has been a promising material for three decades, but the technical difficulties in producing it with low defects have given it a checkered history. Recently, a new process has been developed by Kyocera that seems to be consistently producing a high grade material (Kyocera SN-240) with very low defects, high fracture toughness, low dielectric loss, and very low magnetism.[69]

One of the best engineering thermo-plastics is polyetheretherketone (PEEK) because of its low dielectric loss and excellent chemical, thermal, and dimensional stability at modest cost, but other insulating materials (kel-f, teflon, macor, torlon, vespel, zirconia) are often chosen for specific background or thermal considerations. Fiberglass reinforced composites are also widely used, but they must be cleaned well after machining to remove traces of steel from the tools, and the glass fibers may produce aluminum, silicon, and fluorine background signals. Excellent epoxies are available for securing components and mounting coils, such as Epo-Tek H54,[40] 353ND,[3] and H74F from Epoxy Technology, Inc., Billerica, Massachusetts. Several brands of kel-f and heat-shrink teflon have sufficiently low hydrogenous content for critical proton applications, but experimentation and careful control are necessary. (See *Solid State NMR Probe Design* for more detailed data on probe materials.)

9   THERMAL ENGINEERING

Linewidth and lineshape are often dependent on temperature control and stability.[70] Most commercial probes are intended to operate from -100 to +120^{0}C, but special liquids probes are commercially available for operation from -170 to +500^{0}C, and solids probes are available to cover the range from 90-

1020 K. Temperatures are usually regulated by using a DC resistive heater (designed for minimal magnetic interaction) to heat a gas stream that is directed past the sample.

First-order heat transfer calculations and simple power balance analysis are often sufficient in the probe design. The heater power P_H required to increase the temperature of the gas by δT with specific heat C_p (1041 J/kg K for N_2) and flow rate G (typically 1-2 g/s for MAS probes) is

$$P_H = GC_p\delta T \tag{30}$$

The gas temperature is usually measured with a copper-constantan thermocouple shortly before it reaches the sample, but optical sensors have also been used. Platinum resistors (RTDs) are better in the range from 30-80 K and above 700 K, but in the intermediate range they are not as accurate as the thermocouple unless magnetic-field-dependent corrections are made. They are sometimes used to sense the heater temperature for protection in the event of inadvertent loss of gas flow. The control problems are more difficult than usually encountered elsewhere because of the requirement of precision temperature control of a stream of low specific heat that may encounter large fluctuations in flow rate. Standard PID (proportional-integral-derivative) control algorithms are standard. Dynamic control stability can be further improved by adding a power estimate that is a function of temperature and flow rate. Lead shot has occasionally been used for a thermal ballast because of its high volumetric specific heat, even at low temperatures.

Heat transfer calculations based on simple conduction calculations through thin sheets are often sufficient:

$$P_T = k_T A\delta T/d \tag{31}$$

where P_T is the thermal conduction power (W), k_T is the thermal conductivity (W/m) of the material, A is the area perpendicular to the direction of heat transfer, δT is the temperature difference between the two surfaces, and d is the thickness in the direction of heat transfer. The other common conduction problem is through a thick-walled tube of length h:

$$P_T = \frac{2\pi k_T h\delta T}{\ln(d_o/d_i)} \tag{32}$$

The high Reynolds numbers (often greater than 10^5) that are seen in dewared transfer lines result in very high heat transfer through the bare glass or metal joints unless they are lined internally with plastic tubing, in which case the above equation can be used to estimate these losses.

The extreme temperatures that are sometimes desired [71-73] can make differential thermal expansion responsible for stresses that exceed the rupture limit of one of the components in the probe if not properly designed. However, most of the materials used in NMR probes have high strength. The exceptions, macor and glasses, tolerate high compressive stresses. Hence, even these materials can often be used with plastics in properly designed situations even though their thermal expansions differ widely. Macor is the only commonly used material that may rupture from internal steady state thermal stresses, as its maximum thermal stress temperature ($T_T = S/b_T E$, where S is tensile strength, b_T is thermal expansion coefficient, and E here is Young's modulus of elasticity) and thermal conductivity are both very low.

10 GRADIENT NMR PROBES

By applying magnetic field gradients in three orthogonal directions ($\delta B_z/\delta x$, $\delta B_z/\delta y$, $\delta B_z/\delta z$), it is possible to use NMR to image macroscopic structures, and indeed this has made clinical Magnetic Resonance Imaging (MRI) an important medical diagnostic technique. Obtaining spatial resolution below 0.5 mm on liquid-like samples requires gradients above the 20 mT/m available in most clinical MR machines. Higher gradients are easily obtained by reducing the size of the gradient coils or improving their efficiency. MR microscopy sometimes involves incorporating the gradient coils into wide-bore or narrow-

bore probes along with small rf coils, though most small-animal MR applications are done in horizontal bore magnets.

Single-axis gradients ($\delta B_z / \delta z$) based on Maxwell pairs (sometimes called anti-Helmholtz coils) are much easier to implement in small spaces and are very useful for diffusion experiments using Pulsed Field Gradients (PFG).[74] Similar probes (but with lower gradient strength) are commonly used for most multi-dimensional liquids NMR applications.

Rapid switching of large gradient coils requires high-power audio amplifiers (up to 500 kW in high-field whole-body gradients). Hence, switching efficiency η_s is very important:

$$\eta_s = \frac{\alpha^2 d_S^4 h_S}{\mu_0 L} \tag{33}$$

where α is the gradient gain (T/Am), d_S is the sample diameter, h_S is the sample length, and L is the gradient coil inductance.[75] (The gradient "gain" is sometimes called 'efficiency', but the above dimensionless definition of switching efficiency is more consistent with other efficiency definitions.) The 'fingerprint' design of Schenck et al [76] achieves much higher η_S than earlier Golay coils.

Image linearity has often been described in terms of field linearity – the relative difference between the gradient field and a linear field at the edge of the sample. A better definition for image accuracy is rms local deviation of the gradient from its mean value throughout the sample volume. This has also been called differential linearity. Local deviations below 10%, or field non-linearity below 3%, are generally desired.

When the gradients are switched, eddy currents are induced in the cold radiation shield of the magnet that have long decay times (often many seconds) because of the ultra-low resistivity of copper below 40 K. Active shielding of the gradients greatly reduces the external fields generated by the gradients and permits rapid pulse techniques without excessive decay times or cryogen boiling.[77] Acoustic resonances in the gradient coils may limit gradient recovery time, particularly at very high fields, but novel coil geometries and ceramic formers are useful in addressing this issue.[75, 78] (See also **Gradient Coil Systems,** and **Field Gradients and Their Applications.)**

11   RELATED ARTICLES

Solid State NMR Probe Design; Probes for High Resolution; Spectrometers: A General Overview; Radiofrequency Systems & Coils for MRI & MRS; Sensitivity of the NMR Experiment; Surface and Other Local Coils for In Vivo Studies; Birdcage and other RF Coils for Whole-Body MR; Shimming of Superconducting Magnets; Fourier Transform Spectroscopy.

Biographical Sketch

F. David Doty. *b* 1950. B.A., Physics, 1972, Anderson University, IN, USA, Ph.D., 1983, Physics, University of South Carolina. Began work in NMR under Paul Ellis, 1979. President of Doty Scientific, Inc., 1982-present. Approx. 30 publications and 25 patents. Research interests include rf electronics, NMR probe technology, electromagnetism, manufacturing, turbomachinery, energy conversion cycles, ceramics engineering, acoustics, economics and religions.

Figure Captions

Figure 1.   A 5-turn solenoid.
Figure 2.   Series RLC circuit.
Figure 3.   Parallel RLC circuit.
Figure 4.   Shunt inductive matching circuit.
Figure 5.   Series capacitive matching circuit.
Figure 6.   Double resonance circuit.
Figure 7.   Three typical NMR probes.

REFERENCES

1.   H. J. Schneider and P. Dullenkopf, *Rev. Sci. Instrum.*, 1977, **48**, 68-73.

2.   L. F. Fuks, F. S. C. Huang, C. M. Carter, W. A. Edelstein, and P. B. Roemer, *J. Magn. Reson.*, 1992, **100**, 229-242.

3.   F. D. Doty, G. Entzminger, Y. A. Yang, *Concepts in Magn. Reson.*, **10**(3), 1998, 133-156.

4.   K. Nicolay, K. P. J. Braun, R. A. de Graaf, R. M. Dijkhuizen, and M. J. Kruiskamp, *NMR in Bio-Med.*, 2001, **14**, 94-111.

5.   H. Kovacs, D. Moskau, M. Spraul, *.Mag. Reson. Spect.*, 2005, **46**, 131-255.

6.   F. D. Doty, J. Kulkarni, C. Turner, G. Entzminger, A. Bielecki, *J. Magn. Reson.*, 2006, **182**, 239-253.

7.   F. D. Doty and P. D. Ellis, *Rev. Sci. Instrum.*, 1981, *52* (12), 1868-1875.

8.   C. Hayes, W. Edelstein, J. Schenck, O. M. Mueller, and M. Eash, *J. Magn. Reson.*, 1985, **63**, 622.

9.   G. J. Kost, S. E. Anderson, G. B. Matson, and C. B. Conboy, J. *Magn. Reson.*, 1989, **82**, 238-52.

10.   F. D. Doty, George Entzminger, and C. D. Hauck, *J. Magn. Reson.*, 1999, **140**, 17-31.

11.   B. P. Sutton, L. Ciobanu, X. Zhang and A. Webb, *MRM* , 2005, **54**, 9-13.

12.   R. Haueisen, D. Marek, M. Sacher, F. Kong, K. Ugurbil, S. Junge, Pres. # 80, ESMRMB, Basel, Switzerland, Sept. 2005.

13.   A. Abragam, London, Oxford University Press, Oxford, UK, 1961.

14.   W. G. Clark, *Rev. Sci. Instrum.,* 1964, **35**, 316-33.

15.   R. R. Ernst and W. A. Anderson, Rev. *Sci. Instrum.*, 1966, **37**, 93-102.

16.   M . H. Levitt, "Spin Dynamics", Wiley, 2001.

17.   M. J. E. Golay, N. J. Rumson, 324/0.5, U.S. Pat. 3 569 823, 1971.

18.   H. D. W. Hill and R. E. Richards, J. *Phys. E. Ser. 2*, 1968, **1**, 977-83.

19.   D. G. Gillies in 'Nuclear Magnetic Resonance,' ed. R. K. Harris, Burlington House, London, 1972, Vol 1, pp. 176-180.

20.   J. D. Ellett, M. G. Gibby, U. Haeberlen, L. M. Huber, M. Mehring, A. Pines, and J. S. Waugh, in 'Advances in Magnetic Resonance', ed. J. S. Waugh, Academic Press, New York, 1971, Vol. 5, pp. 117-176.

21.   D. I. Hoult and R. E. Richards, *J. Magn. Reson.*, 1976, **24**, 71-85.

22. 'The ARRL Handbook for the Radio Amateur', ARRL, Newington, CT, USA, 2006, http://www.arrl.org/catalog/9485/ .

23. Wes H. Hayward, "Introduction to Radiofrequency Design", ARRL, Newington, CT, USA, 1995.

24. J. R. Reitz and F. J. Milford, 'Foundations of Electromagnetic Theory', Addison-Wesley, Palo Alto, 1967.

25. J. D. Jackson, 'Classical Electrodynamics', 2nd ed., Wiley, New York, 1975.

26. C.-N. Chen and D. I. Hoult, 'Biomedical Magnetic Resonance Technology', Adam Hilgar, New York, 1989.

27. D. I. Hoult, *Progress in NMR Spectrosc.*, 1978, **12**, 41.

28. F. D. Doty, R. R. Inners, and P. D. Ellis, *J. Magn. Reson.*, 1981, **43**, 399-416.

29. F. D. Doty, T. J. Connick, X. Z. Ni, and M. N. Clingan, *J. Magn. Reson.*, 1988, **77**, 536-549.

30. J. Tropp, *J. Magn. Reson.*, 1989, **82**, 51-62.

31. Q. W. Zhang, H. Zhang, K. V. Lakshmi, D. K. Lee, C. H. Bradley, and R. J. Wittebort, *J. Magn. Reson.*, 1998, **132**, 167-171.

32. J. Stringer and G. Drobny, *Rev. Sci. Instrum.*, 1998, **69**, 9, 3384-3391.

33. F. D. Doty, G. Entzminger, C. Hauck, and J. P. Staab, *J. Magn. Reson.*, 1999, **138**, 144-154.

34. J.B. Miller, B.H. Suits, A.N. Garroway, and M.A. Hepp, *Concepts in Magn. Reson.*, 2000, **12**(3), 125-136.

35. K. R. Minard and R. A. Wind, *J. Magn. Reson.*, 2002, 154, 336-343.

36. H. J. Jakobsen, P. Daugaard, E. Hald, D. Rice, E. Kupce and P. D. Ellis, *J. Magn. Reson.*, 2002, **156**, 152-154.

37. R. W. Martin, E. K. Paulson, and K. W. Zilm, *Rev. Sci. Instrum.*, 2003, **74**, 3045-3061.

38. N. Sinha, C. Grant, C. Wu, A. De Angelis, S. Howell, S. Opella, *J. Magn. Reson.*, 2005, **177**, 197-202.

39. T. M. deSwiet, .*J. Magn. Reson.*, 2005, **174**, 331-334.

40. P. Gorkov, E. Chekmenev, R. Fu, J. Hu, T. Cross, M. Cotton, W. Brey, .*J. Magn. Reson.*, 2006, **181**, 9-20.

41. W. N. Hardy and L. A. Whitehead, *Rev. Sci. Instrum.*, 1981, **52**, 213.

42. F. D. Doty, 324/318, U.S. Pat. 4 710 719, 1987.

43. Y. Li, A. G. Webb, S. Saha, W. W. Brey, C Zachariah, and A. S. Edison, *Magn. Reson. in Chem.,* 2006, **44**, 255-262.

44. W. A. Anderson, "High Q Normal Metal NMR Probe Circuits," presented at the 42nd ENC, Orlando FL, 2001.

45. D. M. Ginsberg and M. J. Melchner, *Rev. Sci. Instrum.*, 1970, **41**, 122.

46. L. C. Maier and J. C. Slater, *J. Appl. Phys.* **23**, 1952, 68.

47. L. F. Fuks and W. A. Anderson, "Perturbation Method for Finding the RF Field on an NMR Probe", Poster presented at ENC in Orlando, 1997.

48. J. Tropp, poster #1646, Presented at 12th ISMRM, Tokyo, 2004.

49. F. D. Doty and S. Shevgoor, "Beating Reciprocity S/N Expectations in Triple-resonance Narrowbore MAS by Cryogenic Cooling of Critical Circuit Components in the OptiMAS Probe", Presented at Rocky Mountain Conf., Denver, 2005, http://www.dotynmr.com/PDF/OptiMAS_ENC05.pdf.

50. D. W. Alderman and D. M. Grant, *J. Magn. Reson.*, 1979, **36**, 447-51.

51. W. W. Brey, A. S. Edison, R. E. Nast, J. R. Rocca, S. Saha, R. S. Withers, *J Magn Reson*, 2006, **179**, 290-293.

52. J. W. Carlson, *J. Magn. Reson.*, 1988, **78**, 563-73.

53. A. Macovski, *Magn. Res. in Med.,* 1996, **36**, 494-7.

54. W. A. Edelstein, J. F. Schenck, O. M. Mueller, and C. E. Hayes, 324/318, U.S. Pat. 4 680 548, 1987.

55. S. M. Holl, R. A. McKay, T. Gullion, and J. Schaefer, *J. Magn. Reson.*, 1990, **89**, 620-6.

56. F. D. Doty, 324/322, U.S. Pat. 5 162 739, 1992.

57. E. Najim and J-P Grivet, J. *Magn. Reson.*, 1991, **93**, 27-33.

58. J. R. Fitzsimmons, H. R. Brooker, and B. Beck, *Magn. Reson. Med.*, 1989, **10**, 302-309.

59. F. D. Doty, G. Entzminger, J. Kulkarni, L. Li, J. P. Staab, "RF Coil Technology for Small-Animal MRI", *NMR in Biomedicine*, in press.

60. F. D. Doty, S. Shevgoor, J. B. Spitzmesser, "Progress on 4-channel 3 mm CryoMAS Probe with Auto Sample Exchange for High-field Solids NMR", Presented at EuroMAR, York, UK, 2006.

61. J. A. Stringer, C. E. Bronnimann, C. G. Mullen, D. H. Zhou, S. A. Stellfox, Y. Li, E. H. Williams, C. M. Rienstra, *J. Magn. Reson.*, 2005, **173**, 40-48.

62. F. D. Doty, Y. A. Yang, and G. E. Entzminger, 1998, **10**(4), 239-260.

63. F. D. Doty and G. Entzminger J., "Thermal Buffering of Cross-Coils in High-Power NMR Decoupling," U.S. Pat. 6 320 384, 2001.

64. H. D. Hill, A. P. Zens, 324/318, U.S. Pat. 4 517 516, 1985.

65. H. D. Hill, U.S. Pat. 4 563 648, 1986.

66. M. Hansen, ed., 'Constitution of Binary Alloys', 2nd. edn., McGraw-Hill, New York, 1989.

67. J. R. Davis (ed.), 'Metals Handbook', 10th Edn., Vol. 2, ASM International, Materials Park, OH, 1990.

68. M. L. Buess and G. L. Petersen, *Rev. Sci. Instrum.*, 1978, **49**, 1151-5.

69. Kyocera materials data, http://global.kyocera.com/prdct/fc/product/pdf/material_e.pdf , 2005.

70. A. Allerhand and S. R. Maple, *J. Magn. Reson.*, 1988, **76**, 375-9.

71. F. D. Doty, J. B. Spitzmesser, and D. G. Wilson, U.S. Pat. 5 202 633, 1993.

72. M. S. Conradi, *Concepts in Magn. Reson.*, 1993, **5**, 243-62.

73. A. M. George, J. F. Stebbins, *Am. Mineralogist*, 1995, **80**, 878-884.

74. P. T. Callaghan and Y. Xia, *J. Magn. Reson.*, 1991, **91**, 326-52. (Important improvements in the original technique have been developed: D. Wu, A. Chen, and C. S. Johnson, *J. Magn. Reson., Ser. A,* 1995, **115**, 260.)

75. F. D. Doty, "Optimization of MRI Gradient Coils" in *Spatially Resolved Magnetic Resonance*, Ed. by P. Blumler, B. Blumich, R. E. Botto, and E. Fukushima, Wiley-VCH, Weinheim, 1998.

76. J. F. Schenck, M. A. Hussain, W. A. Edelstein, 324/318, U.S. Patent 4 646 024, 1987.

77. P. Mansfield and B. Chapman, *J. Magn. Reson.,* 1986, **66**, 573-576.

78. R. Bowtell and P. Mansfield, *Magn. Reson. Med*., 1995, **34**, 494.